

ENVIRONMENTAL RESEARCH
LETTERS

OPEN ACCESS

RECEIVED
9 May 2022REVISED
30 August 2022ACCEPTED FOR PUBLICATION
3 October 2022PUBLISHED
12 October 2022

Original Content from
this work may be used
under the terms of the
[Creative Commons
Attribution 4.0 licence](#).

Any further distribution
of this work must
maintain attribution to
the author(s) and the title
of the work, journal
citation and DOI.



LETTER

Downwind control of oceanic air by land: the land wake and its sensitivity to CO₂Marysa M Laguë^{1,2,*} , Gregory R Quetin³ and William R Boos^{4,5} ¹ Coldwater Lab, Center for Hydrology, University of Saskatchewan, Canmore, AB, Canada² Department of Atmospheric Sciences, University of Utah, Salt Lake City, UT, United States of America³ Department of Geography, University of California, Santa Barbara, CA, United States of America⁴ Department of Earth and Planetary Science, University of California, Berkeley, Berkeley, CA, United States of America⁵ Climate and Ecosystem Sciences Division, Lawrence Berkeley National Laboratory, Berkeley, CA, United States of America

* Author to whom any correspondence should be addressed.

E-mail: marysa.lague@usask.ca**Keywords:** climate, land-ocean interactions, land-atmosphere interactions, advection, energy, cloudsSupplementary material for this article is available [online](#)**Abstract**

Oceans are well-known to be directly altered by global climate forcings such as greenhouse gas changes, but how oceans are indirectly influenced by land and its response to such forcings remains less explored. Here, we assess the present-day and projected future state of a little-explored feature of the climate system—a ‘land wake’ in relative humidity downwind of the east coast of North America, consisting of low-humidity continental air extending roughly 1000 km over the Atlantic ocean. The wake exists throughout the year, but is supported by high continental temperatures in summer and low continental moisture in winter. The wake is well represented in an ensemble of global climate models (GCMs), qualitatively matching reanalysis data. Under increasing atmospheric CO₂, the land wake intensifies in GCM simulations through two pathways: the radiative effects of CO₂ on surface temperatures, and the biogeochemical effect of CO₂ on terrestrial vegetation. Vegetation responses to increased CO₂ alter the summer wake from Florida to Newfoundland, and both the radiative and biogeochemical effects of CO₂ drive reductions in coastal cloud cover. These changes illustrate the potential of rapidly changing terrestrial climate to influence coastal regions and the ocean environment downwind of continents through both light conditions and the energy balance of the surface ocean.

1. Introduction

Differences in the surface properties of ocean and land produce large asymmetries in the interaction of these two components of the climate system with the overlying atmosphere. Oceans have a large heat capacity and slow dynamics (Cess and Goldenberg 1981, North *et al* 1983), which allow years-long variations in sea surface temperature to drive atmospheric circulations that influence climate in remote continental regions (Myneni *et al* 1966, Yang and Delsole 2012, Perry *et al* 2017). Land lacks sufficient heat capacity to create such persistent thermal forcings, but continents alter the atmosphere mechanically, e.g. by generating orographic stationary waves that dominate the northern hemisphere circulation in winter (Cook and Held 1992, Held *et al* 2002, Maroon

et al 2015, White *et al* 2017), and by generating seasonal thermal forcings such as those that drive cross-equatorial monsoon circulations (Li and Yanai 1996, Wu *et al* 2012, Boos and Kuang 2013). In this study, we quantify and explore the mechanisms governing a little-explored feature of the climate system—a ‘land wake’ consisting of maritime air that has been perturbed by the passage of prevailing winds over a continent.

We are motivated by the fact that land and ocean influence each other by serving as sources for tracers that are carried by winds. Oceans serve as the primary source of moisture and of pristine, unpolluted air for continents (Parrish and Hahn 1992, Robertson *et al* 2016). Past studies have examined how continental air masses that are transported over ocean transform the aerosol content of the marine boundary layer (Fuchs

et al 2017, Fu *et al* 2018), influencing cloud properties over ocean (Garrett and Hobbs 1995, Fuchs *et al* 2017). Seasonal differences in high-latitude cold air outbreaks impact the seasonality of aerosol nucleation (Nilsson *et al* 2001). Outbreaks of dry and dusty air from the Sahara have been shown to episodically alter the thermal structure and likelihood of tropical cyclogenesis over the Atlantic (Carlson and Prospero 1972). As polar continental air transitions to polar maritime air, its moisture content increases due to ocean evaporation, altering both the temperature and moisture content of the air mass (Burke 1945). Movement of air masses between continental and maritime regions is responsible for numerous weather phenomenon including cold air outbreaks and high-latitude cyclogenesis (Businger and Reed 1989, Pithan *et al* 2018). The larger diurnal temperature cycle of land drives land-sea breezes (Sonu *et al* 1973, Gannon 1978, Gille *et al* 2005).

The fact that source regions, such as continents, can imprint themselves on the thermodynamic state of air motivated Bergeron's widely used air mass classification system (Bergeron 1930) and its modifications, e.g. for the Americas (Willett 1933). Such systems generally classify air as being either continental or maritime in origin, and also polar or tropical in origin, motivated by the recognition that transient extratropical cyclones mix air meridionally (Palmén 1951). Such classification was often qualitative and subjective, but numerical objective approaches have been used (Schwartz 1991, Kalkstein *et al* 1996) and secular trends in air mass characteristics have been analyzed in some limited regions (Schwartz 1995). Nevertheless, the mechanisms by which land masses alter the seasonal cycle of downwind oceanic air remain poorly quantified, particularly in the midlatitudes where the jet stream is expected to routinely transport continental air eastward over the Atlantic and Pacific ocean basins.

Understanding the influence of land on the climatological mean state of oceanic air is particularly important given ongoing changes in continental states. Changes in the land surface alter the climate both locally and globally (Bathiany *et al* 2010, Davin *et al* 2010, Kooperman *et al* 2017, Laguë *et al* 2019); large changes in vegetation can drive atmospheric change over both land and ocean regions through atmospheric teleconnections and shifts in atmospheric circulation (Bonan *et al* 1992, Bonan 2008, Swann *et al* 2012, Laguë and Swann 2016). In terrestrial regions with strong land-atmosphere coupling, changes in soil moisture and vegetation drive changes in precipitation (Koster *et al* 2006).

The low heat capacity and relative dryness of land causes land to have a large temperature response to thermal forcings, as evidenced by both the increased variance of land temperature (e.g. seasonally) and the amplified response of land to heating from increased

atmospheric CO₂ (Sutton *et al* 2007, Fu and Feng 2014, Hartmann 2016, Chadwick *et al* 2019). While increased atmospheric CO₂ over oceans decreases outgoing longwave radiation there, CO₂ increases over land lead to circulation responses which move atmospheric energy from continental to oceanic regions (Shaw and Voigt 2016). Plant responses to CO₂, changes in soil moisture, growing season timing and length changes, and changes in snow pack lead to further amplification of continental warming with increased atmospheric CO₂ (Campbell *et al* 2005, Dong *et al* 2009, IPCC 2022).

Here we ask how land influences the seasonal mean state of oceanic air downwind of a continent, using the particular case of the Atlantic Ocean east of North America; this coastal region is home to numerous large population centers and regions of high marine productivity. We examine this remote influence of land in the present climate and in projections of changes resulting from the distinct impacts of CO₂ on atmospheric radiation and on plant physiology.

2. Methods

2.1. The land wake

We define the 'land wake' W_x of some variable x as the deviation from the zonal mean value of x of air over the ocean ($[x_{\text{ocean}}]$) at a given latitude (equation (1)).

$$W_x = x - [x_{\text{ocean}}] \quad (1)$$

W_x can be calculated globally or for a single ocean basin, at any atmospheric level. We focus on the near-surface wake averaged from 1000–900 hPa (the precise shape of the wake varies depending on the vertical levels selected), downwind of mid-latitude North America, where $[x_{\text{ocean}}]$ is averaged longitudinally over the Atlantic ocean, defined here to be the ocean region between 100° W–0° W and 20° N–70° N. $W_x < 0$ indicates x at that location is smaller than the average oceanic value of x for that latitude, while $W_x > 0$ indicates x is larger than the average oceanic value of x for that latitude. In this study, we focus on the wakes of relative humidity (W_{RH}), specific humidity (W_Q), and temperature (W_T).

2.2. Climate data

We analyse the land wake using a combination of reanalysis data and climate model output. We use the ERA5 reanalysis global dataset at 0.25° resolution, which spans from 1979–2019 (Hersbach *et al* 2020). Specifically, we use the ERA5 variables for: relative humidity (RH), specific humidity (q), temperature (T), and winds (U, V).

We also evaluate the wake in Earth system models under low and high atmospheric CO₂ concentrations. Increased atmospheric CO₂ has both radiative and biological impacts. These effects are isolated in a pair of experiments from the Coupled

Climate-Carbon Cycle Model Intercomparison Project (C4MIP Friedlingstein *et al* 2006, Jones *et al* 2016). In ‘1pctCO₂-bgc’, only the biogeochemical (bgc) components of the models experience CO₂ increasing at 1% per year from pre-industrial values (280 ppm), while the atmosphere experiences constant pre-industrial CO₂. In ‘1pctCO₂-rad’, only the atmospheric radiation experiences increasing CO₂ (at 1% per year), while the biogeochemical components of the model experience fixed pre-industrial CO₂. We also consider simulations from the ‘1pctCO₂’ experiment from the Coupled Model Intercomparison Project v. 6 (Eyring *et al* 2016), where both radiation and biogeochemistry experience the increase in CO₂. Simulations are run for 140 years, at which point CO₂ concentrations reach 4x pre-industrial levels (figure S1). We refer to the increase in CO₂ experienced by the biogeochemistry as bgcCO₂, the increase in CO₂ experienced by the atmospheric radiation as radCO₂, and use fullCO₂ to refer to simulations where both biogeochemistry and radiation experience increased CO₂.

Both the terrestrial and oceanic carbon cycles experience the increase in bgcCO₂, but impacts on surface fluxes are only driven by the response of terrestrial vegetation to increased CO₂. The bgcCO₂ simulations thus provide a clear demonstration of changes in land driving changing conditions over the ocean in the land wake. At higher CO₂ concentrations, plants can grow more (CO₂ fertilization; Field *et al* 1995, Sellers *et al* 1996, Medlyn *et al* 2001, Morison 2001), altering leaf area and land albedo, in turn leading to changes in surface temperatures and evapotranspiration (Donohue *et al* 2013, Swann *et al* 2016, Zariski *et al* 2020a). Atmospheric CO₂ concentrations directly impact the stomatal conductance of vegetation. In global Earth system models, the equations governing stomatal conductance generate less conductance (thus less evapotranspiration, with all else held equal) with increased atmospheric CO₂ concentrations (Ball *et al* 1987, Medlyn *et al* 2011), changing plants’ water use efficiency (Eamus 1991, Cheng *et al* 2014).

The effect of the biogeochemical response to increased CO₂ could be obtained by considering results from high-low CO₂ values in the bgcCO₂ simulations, or by subtracting the radCO₂ simulation from the fullCO₂ simulation. The first gives the effect of increasing bgcCO₂ in a low-CO₂ climate, while the latter gives the effect of increasing bgcCO₂ in a high-CO₂ climate; we focus on the first approach in this study, but show that the two methods give generally qualitatively similar responses of the land wake.

We use the nine models participating in C4MIP that provided temperature, specific humidity, and RH data for the 1pctCO₂-bgc and 1pctCO₂-rad C4MIP experiments and were available for download

from the LLNL ESGF node (<https://esgf-node.llnl.gov/projects/cmip6/>) on 11 August 2021 (table 1). These models were BCC-CSM2-MR, CanESM5, CNRM-ESM2-1, ACCESS-ESM1-5, IPSL-CM6A-LR, MIROC-ES2L, UKESM1-0-LL, MPI-ESM1-2-LR, and CESM2. Cloud cover data was available for all models except CanESM5, so low cloud and downwelling solar radiation are evaluated for the remaining eight models only; snow cover and leaf area changes are shown for all models except CanESM5 and BCC-CESM2-MR as neither model had both variables available. Where possible, the r1i1p1f1 ensemble member was used, otherwise the r1i1p1f2 ensemble member was used; only a single ensemble member per model was considered. All output was re-gridded to a common 1° resolution horizontal grid. For each field considered, we took the difference of the average of years 121–140 (high CO₂) and subtracted the average of years 1–20 (low CO₂).

2.3. Wake magnitude

To compare changes in the RH wake in the C4MIP simulations with increased bgcCO₂ and radCO₂, we define the ‘magnitude’ M of the wake as the area-weighted sum of the spatial footprint of the Atlantic RH wake, in this case, anywhere RH < 0, multiplied by the intensity of the wake W_{RH} , where W_{RH} is how negative RH is at each location:

$$M_{RH, \text{Atlantic}} = \frac{\int_{105^{\circ}W}^{25^{\circ}W} \int_{25^{\circ}N}^{65^{\circ}N} (\cos \phi W_{RH}) |_{W_{RH} < 0} d\phi d\lambda}{\int_{105^{\circ}W}^{25^{\circ}W} \int_{25^{\circ}N}^{65^{\circ}N} (\cos \phi) |_{W_{RH} < 0} d\phi d\lambda}, \quad (2)$$

where ϕ is the latitude. $M_{RH, \text{Atlantic}}$ is calculated using W_{RH} in the domain 25–65° N and 105–25° W, only where W_{RH} is negative.

We take the difference of the average monthly $M_{RH, \text{Atlantic}}$ of years 121–140 (high bgcCO₂ and radCO₂) minus the average monthly $M_{RH, \text{Atlantic}}$ of years 1–20 (low bgcCO₂ and radCO₂) for the 1pctCO₂-bgc and 1pctCO₂-rad simulations, respectively. We similarly calculate the change in continental RH (averaged over land areas from 1000 to 90 hPa, between 25°–65° N and 125°–55° W) for each month of the year, then take seasonal averages. The wake area changes slightly with increasing bgcCO₂ and radCO₂ (table S1), but most of the change in the wake magnitude comes from changes within the climatological wake footprint.

2.4. Wake intensity

To evaluate the individual contributions of T and q to the change in W_{RH} , we define an additional metric, the change in the wake ‘intensity’ (equation (3)). I_{RH} is calculated in the box 25°–65° N and 105°–25° W, only where $\Delta W_{RH} < 0$ (see figure 3) for each individual model. Within that footprint, a similar

Table 1. C4MIP model simulations used in this study, with data downloaded from the LLNL ESGF node (<https://esgf-node.llnl.gov/projects/cmip6/>) on 11 August 2021. Variables used are: downwelling shortwave radiation (rsds), cloud fraction (cl), winds (ua, va), atmospheric temperature (ta), specific humidity (hus), relative humidity (hur), snow amount (snw), and leaf area index (tai).

Modeling center	Model name	1pctCO2-bgc ensemble member	1pctCO2-rad ensemble member	Variables assessed
Beijing Climate Center (BCC)	BCC-CSM2-MR	r1i1p1f1	r1i1p1f1	rsds, cl, ua, va, ta, hus, hur
Canadian Centre for Climate Modeling and Analysis (CCCma)	CanESM5	r1i1p1f1	r1i1p1f1	ua, va, ta, hus, hur
Centre National de Recherches Météorologiques (CNRM-CERFACS)	CNRM-ESM2-1	r1i1p1f2	r1i1p1f2	rsds, cl, ua, va, ta, hus, hur, snw, tli
Commonwealth Scientific and Industrial Research Organization (CSIRO)	ACCESS-ESM1-5	r1i1p1f1	r1i1p1f1	rsds, cl, ua, va, ta, hus, hur, snw, tli
Institut Pierre Simon Laplace (IPSL)	IPSL-CM6A-LR	r1i1p1f1	r1i1p1f1	rsds, cl, ua, va, ta, hus, hur
Model for Interdisciplinary Research on Climate (MIROC)	MIROC-ES2L	r1i1p1f2	r1i1p1f2	rsds, cl, ua, va, ta, hus, hur, snw, tli
Max Planck Institute for Meteorology (MPI-M)	MPI-ESM1-2-LR	r1i1p1f1	r1i1p1f1	rsds, cl, ua, va, ta, hus, hur, snw, tli
Met Office Hadley Centre (MOHC)	UKESM1-0-LL	r1i1p1f2	r1i1p1f2	rsds, cl, ua, va, ta, hus, hur, snw, tli
National Center for Atmospheric Research (NCAR)	CESM2	r1i1p1f1	r1i1p1f1	rsds, cl, ua, va, ta, hus, hur, snw, tli

approach is used as with the calculation of the magnitude M_{RH} , i.e. taking the area-weighted sum of the wake values in that region (but only where the wake changes, i.e. where $\Delta W_{RH} < 0$).

$$I_{RH} = \frac{\int_{105^W}^{25^W} \int_{25^N}^{65^N} (\cos \phi W_{RH}) |_{\Delta W_{RH} < 0} d\phi d\lambda}{\int_{105^W}^{25^W} \int_{25^N}^{65^N} (\cos \phi) |_{\Delta W_{RH} < 0} d\phi d\lambda}, \quad (3)$$

To separate the impact of T and q on W_{RH} , ΔW_{RH} , and I_{RH} , we calculate W_{RH} in three distinct ways. First, we calculate W_{RH} in the standard manner (equation (1)). Second, we calculate what the RH field would be in the high CO₂ case if we hold q fixed to the low CO₂ value, but increase T to the high CO₂ value; we then calculate the wake of that new RH value that only accounts for the change in T . Third, we calculate what the RH field and W_{RH} would look like with high CO₂ if only q is increased to high CO₂, with T held to the low CO₂ value. I_{RH} can then be calculated within the ΔW_{RH} footprint for low CO₂ (using W_{RH} at low CO₂), for RH associated with low CO₂ q and high CO₂ T , for RH associated with low CO₂ T and high CO₂ Q , and for RH at high CO₂. These terms do not add linearly as RH is not a linear function of T and q and we approximate the effect of ΔT and Δq on ΔRH using monthly mean T and q values. The actual change in RH is qualitatively similar but numerically differs slightly from the change in RH calculated from monthly mean T and q together (not shown).

2.5. Analysis tools and details

From equation (1), changes in the wake W_x could occur either because of a change in the spatial pattern of x , or because of a change in the zonal mean of x averaged over the Atlantic basin. In the case of increased bgcCO₂, the changes in the RH wake are driven by spatial changes in RH off the North American east coast, with very little change in the zonal mean value of RH over the Atlantic ocean. This is not surprising, as bgcCO₂ primarily impacts surface energy and water fluxes over the continents; this signal is then advected over the ocean and thus is strongest in the wake region, with very little change in the average Atlantic RH at each latitude (figure S2).

Increasing radCO₂ has a strong impact on the atmospheric radiative budget and surface temperatures over both land and ocean regions, causing the zonal mean Atlantic values of T and q to increase, but zonally averaged RH over the ocean remains roughly the same (O'Gorman and Muller 2010). Regionally however, RH and the RH wake become drier with increasing radCO₂ off the North American east coast, as a result of continental warming (figure S3).

Western boundary currents, such as the Gulf Stream, cause a tongue of anomalously warm water extending into cooler waters at higher latitudes along the east coast of mid-latitude continents, releasing heat and moisture to the atmosphere above it. In the context of our definition of the wake, this would

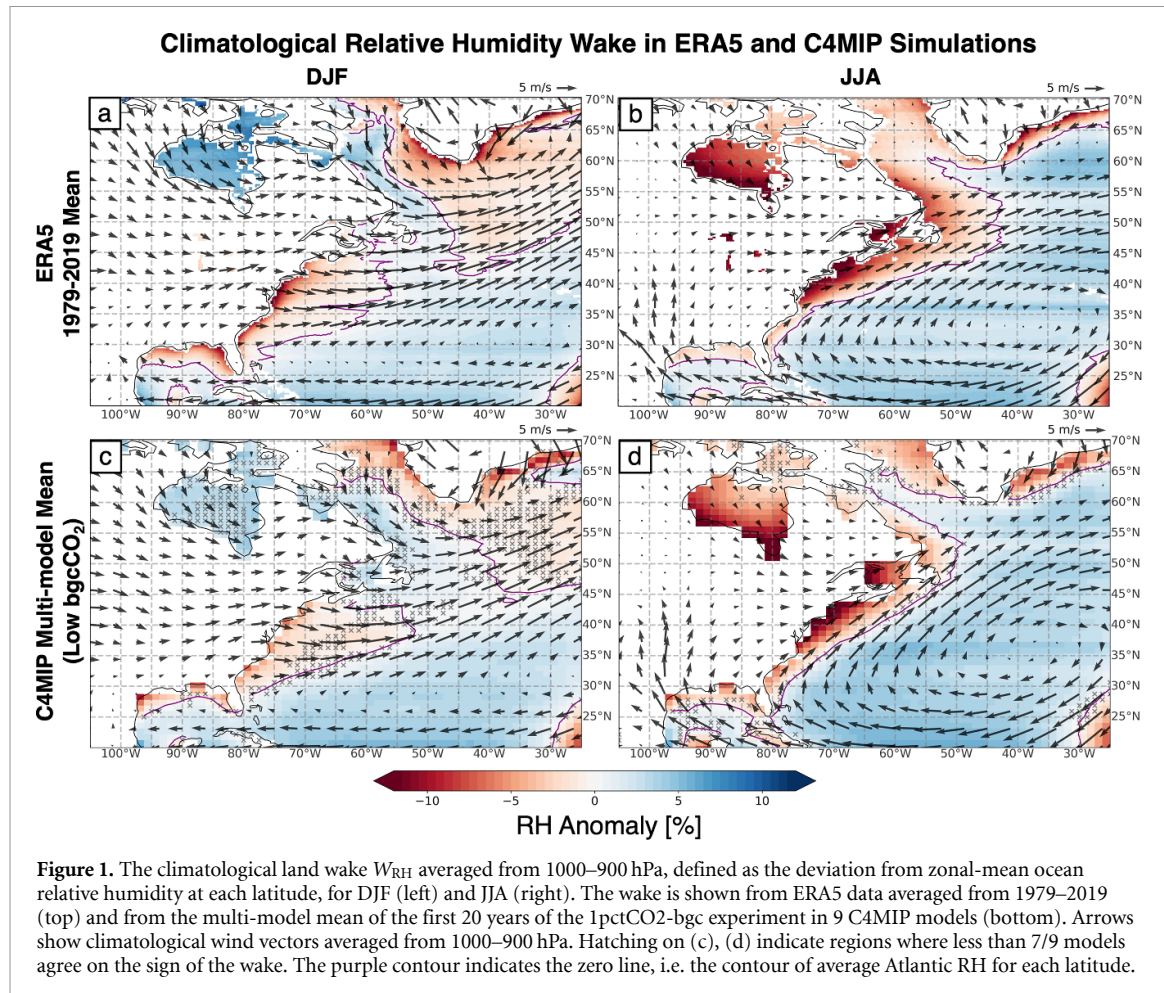


Figure 1. The climatological land wake W_{RH} averaged from 1000–900 hPa, defined as the deviation from zonal-mean ocean relative humidity at each latitude, for DJF (left) and JJA (right). The wake is shown from ERA5 data averaged from 1979–2019 (top) and from the multi-model mean of the first 20 years of the 1pctCO₂-bgc experiment in 9 C4MIP models (bottom). Arrows show climatological wind vectors averaged from 1000–900 hPa. Hatching on (c), (d) indicate regions where less than 7/9 models agree on the sign of the wake. The purple contour indicates the zero line, i.e. the contour of average Atlantic RH for each latitude.

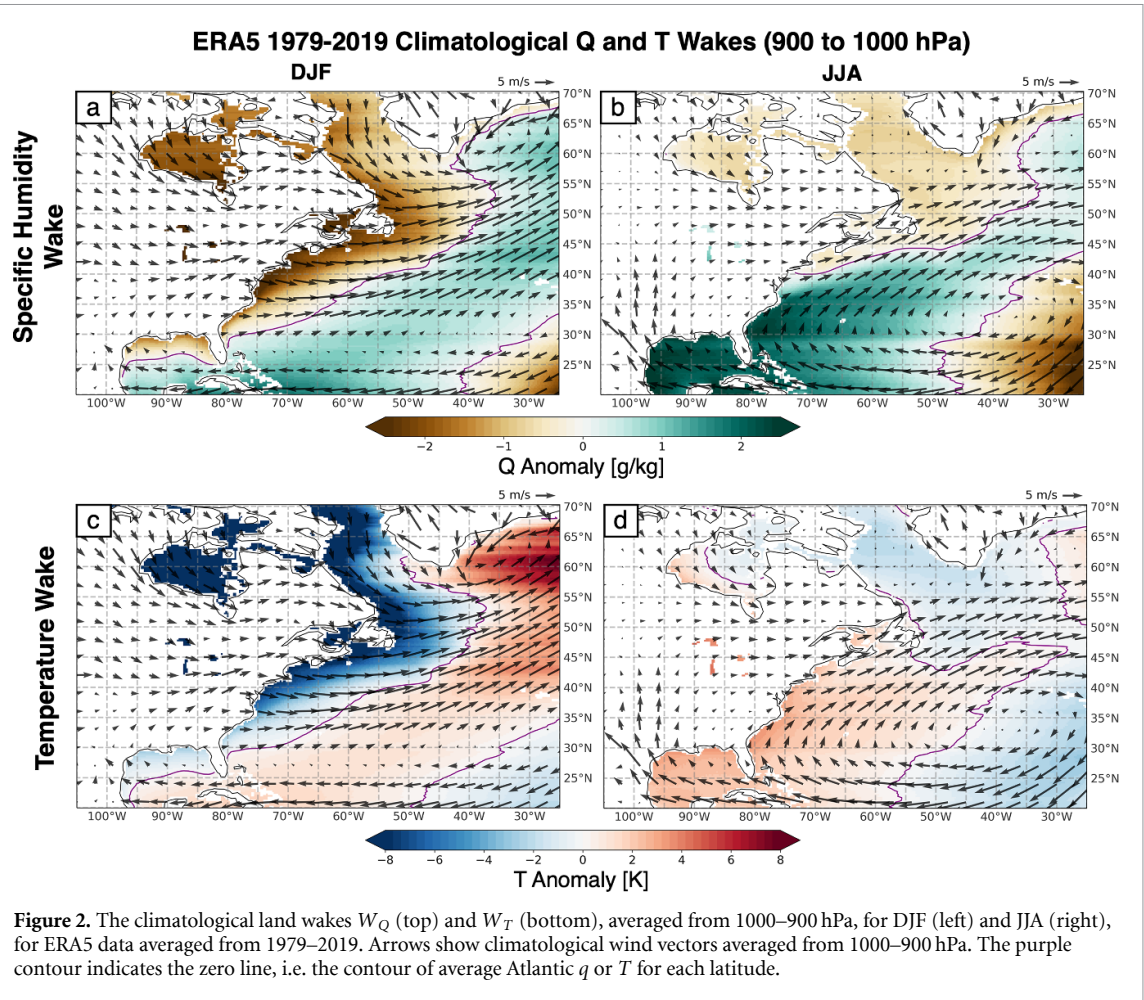
raise the overall zonally averaged RH, T , and q of the ocean basin. As such, air that is near the coast but has not yet reached the eastern boundary current could look anomalously cold or dry simply because it has not yet come into contact with the warmer waters. The C4MIP simulations analyzed here show that the RH, T , and q of the wake region change in response to increased bgcCO₂ and radCO₂—that is, even if the wake only existed as an artifact of the eastern boundary currents, our analysis still shows the sensitivity of oceanic air in this region to terrestrially-driven changes in continental air. Changes in the location and strength of the Gulf Stream, e.g. with changing climate, could alter both the shape and strength of the continental wake by modifying wind patterns and ocean-atmosphere exchange of heat and moisture. For example, a warmer gulf stream could potentially reduce the continental wake as increased ocean evaporation could more quickly make continental air resemble ocean air.

Analysis was conducted using the Python programming language, heavily leveraging the NumPy (Harris *et al* 2020) and xarray (Hoyer and Hamman 2017) packages.

3. Results

3.1. The present-day land wake and its causes

In reanalysis data, W_{RH} downwind of mid-latitude North America is negative in both winter (December–February, DJF) and summer (June–August, JJA), becoming positive as air moves further from shore (figures 1(a) and (b)); that is, air near the continent has a lower RH than air farther from land. The shape of the wake changes with season, but its longest dimension is generally aligned parallel to the time-mean low-level wind with a peak length of at least 1000 km. In winter, W_{RH} extends from the northern coast of the Gulf of Mexico along the eastern seaboard of the USA to around 50° N, with an additional region of anomalously low RH around Greenland (figure 1(a)). In summer, the wake lies closer to shore along the east coast of the USA, but extends further north along the east coast of Canada and Hudson Bay, while the Greenland wake retreats towards the coast of that land mass (figure 1(b)). Eastward winds off the continent are stronger in winter, and the winter wake correspondingly extends farther from shore between 30°–45° N. In contrast, the summer



wake is more intense and occupies a larger fraction of the coastline of North America.

While the RH wake is apparent in both winter and summer, it is driven by different mechanisms seasonally. In winter, cold, dry air flows from the continent over ocean, producing low temperature (T) and low specific humidity (q) offshore (figures 2(a) and (c)). However, because saturation vapor pressure decreases rapidly as temperature drops, the low temperatures in more northern regions prevent anomalously low RH downwind of the continent. The winter wakes in T and q extend along nearly the entire coastline of North America, but their interaction limits the RH wake to latitudes south of Nova Scotia (figure 1(a)). In summer, time-mean winds along eastern North America flow more parallel to the coast due to the summertime anticyclone over the Atlantic (figure 1(b)). At more southern latitudes, q is anomalously positive due to moisture transport from the low-latitude ocean, while at more northern latitudes q is anomalously negative where there is flow off the continent (figure 2(b)). Close to the continent, air is warmer than average ocean air (figure 2(d)); as in winter, the shape of W_{RH} results from the strong response of saturation vapor pressure to temperature, yielding low RH along the whole east coast of North

America despite anomalously high q south of 40° N (figures 1(b) and 2(b)).

Mixing between continental and maritime regions produced by shorter timescale motions and vertical circulations is likely also a factor in determining the wake. For example, along the northern coast of the Gulf of Mexico, monthly mean winds are climatologically onshore, yet a distinct band of low RH air hugs the coast. The difference in seasonal drivers of W_{RH} illustrate the potential for long-term changes to land, such as those caused by agriculture, fire, drought, and rising atmospheric CO₂, to impact ocean regions downwind of continents through multiple mechanisms.

3.2. Intensification of the land wake by increased CO₂

Temperature increases due to climate change are occurring more quickly over land than over most ocean regions (IPCC 2007), and the existence of the land wake provides a pathway for land's response to climate change to influence ocean regions. Earth System Models (ESMs) participating in C4MIP produce a qualitatively similar W_{RH} to that seen in reanalysis (cf top and bottom rows of figure 1), with the ERA5

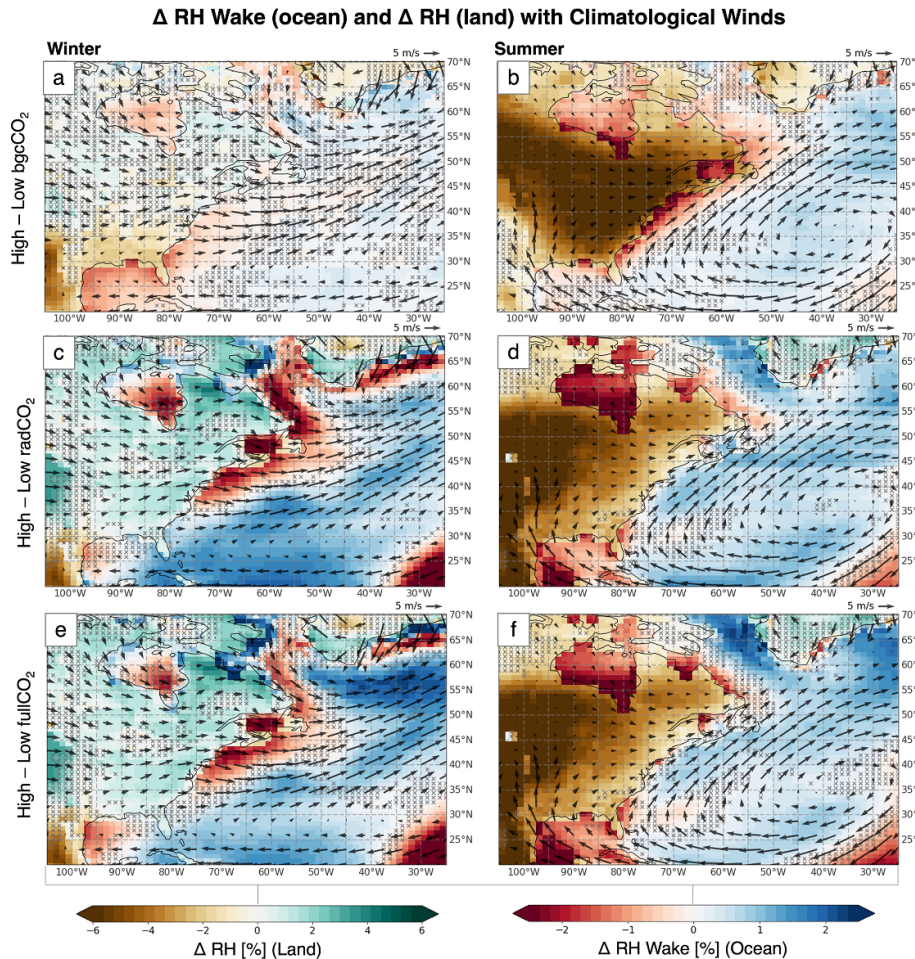


Figure 3. Change (high—low CO₂) in the RH land wake for the difference of the end-start of the C4MIP simulations where only the carbon cycle sees increased bgCO₂ (top), only radiation sees increased radCO₂ (middle), and both bgc and radiation see increased CO₂ (bottom) for winter (DJF, left) and summer (JJA, right). Negative values indicate a ‘drying’ (lower RH) of the wake. Hatching indicates where less than 7/9 models agree on the sign of the response. The change in RH [%] is shown over land, with change in the RH Wake [%] over the ocean. Wake values and continental RH are averaged from the surface to 900 hPa. Vectors show climatological winds averaged from 1000 to 900 hPa.

wake having a slightly larger area than the models (table S1).

Increases in bgCO₂ and radCO₂ each separately strengthen the land wake (figure 3). The spatially integrated magnitude of the RH wake ($M_{RH, \text{Atlantic}}$, see section 2) intensifies in response to both increased bgCO₂ and radCO₂, with both driving similar magnitudes of change in $M_{RH, \text{Atlantic}}$ during summer (figures 4(a) and (b)). This intensification of the wake accompanies a large reduction of RH over continental North America during spring, summer, and autumn (figure 4), although the spring and autumn changes are less pronounced in the radCO₂ experiment. There is a strong correlation across models ($r^2 = 0.72$) between the change in RH over North America and the change in the RH wake magnitude associated with increased bgCO₂, and a more modest correlation ($r^2 = 0.57$) for radCO₂. These results support the hypothesis that changes in continental air induced by the radiative and biogeophysical effects of CO₂ drive changes in the wake.

When radiative and biogeophysical effects of CO₂ are both considered (using the fullCO₂ simulations), the radCO₂ effects are seen to dominate the spatial pattern of change in the wake found in the fullCO₂ simulation (figure 3). However, the effects of bgCO₂ contribute substantial changes to the wake magnitude (figure 4(c)). We would not expect the wake changes in the bgCO₂ and radCO₂ simulations to sum perfectly linearly to the fullCO₂ wake change because the results of the ΔbgCO₂ simulations show the effect of bgCO₂ in a low-CO₂ background climate, while the difference between the fullCO₂ and radCO₂ simulations show the effect of bgCO₂ in a high-CO₂ background climate. However, the full—rad wake response is qualitatively similar to the bgCO₂ wake response in most regions, except in the Hudson Bay and Davis Straight areas (figures S4–S6). These differences are not the focus of our study, but we suspect they result from large differences in base-state Arctic climate with low vs. high CO₂.

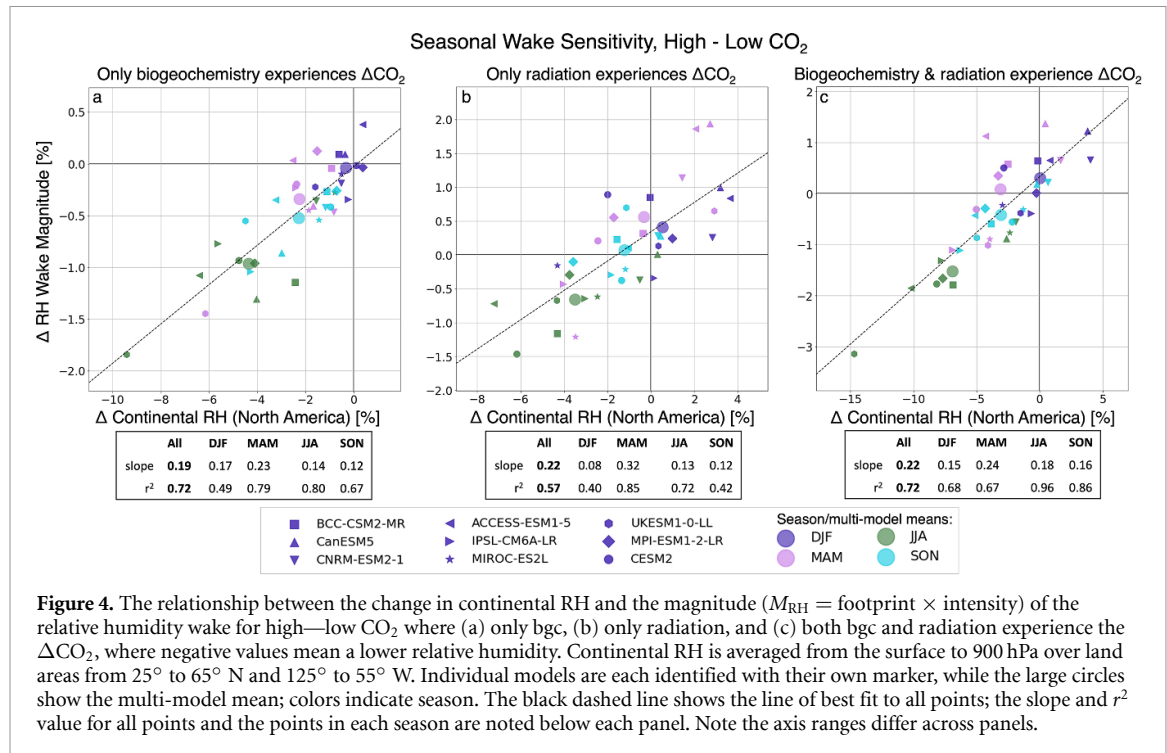


Figure 4. The relationship between the change in continental RH and the magnitude (M_{RH} = footprint \times intensity) of the relative humidity wake for high—low CO_2 where (a) only bgc, (b) only radiation, and (c) both bgc and radiation experience the ΔCO_2 , where negative values mean a lower relative humidity. Continental RH is averaged from the surface to 900 hPa over land areas from 25° to 65° N and 125° to 55° W. Individual models are each identified with their own marker, while the large circles show the multi-model mean; colors indicate season. The black dashed line shows the line of best fit to all points; the slope and r^2 value for all points and the points in each season are noted below each panel. Note the axis ranges differ across panels.

3.3. Biogeophysical effects of CO_2 intensify wake through stomatal closure

We now focus on how the response of terrestrial evapotranspiration to increased bgcCO_2 impacts the wake. The summer response across the C4MIP simulations to increased bgcCO_2 is a widespread reduction in terrestrial evapotranspiration (figure S7). The terrestrial biogeophysical effects of increased CO_2 produce a wake that is drier (i.e. W_{RH} is anomalously low) over the coastal ocean in both summer and winter with increased bgcCO_2 (figures 3(a) and (b)). Note that though the RH wake becomes drier, specific humidity in the summer wake actually increases because of circulation changes, discussed below. While the horizontal extent of this change in the wake is smaller in summer, the peak intensity (defined by equation (3)) of this change is larger during that season. Although the definition of W (equation (1)) encompasses the whole Atlantic, the change in W_{RH} is primarily the result of changes near North America, with little influence from the zonal-mean change (figures S2, S7; see section 2 for further discussion).

In summer, continental RH decreases as a result of reduced continental evapotranspiration driven by the stomatal response to increased bgcCO_2 , but the influence of these continental changes on the RH wake is more complex than a simple downwind transport of low-RH air. The reduced continental evapotranspiration causes lower continental q as well as higher continental T due to reduced latent cooling of land (see land regions in figures 3(b) and

S7((b), (d)). Downwind transport of high- T air over the wake region drives an intensification of the RH wake, but this is partially opposed by an increase in q over much of the western Atlantic (figures S7(b) and (d)). Because continental q decreases with increased bgcCO_2 , the downwind transport of lower q continental air cannot explain the summer increase in q in the wake region. Summer ocean evaporation also does not change substantially in the wake region (figure S8). Instead, the increase in summer q over the western Atlantic is due to a change in atmospheric circulation. The continental warming resulting from reduced evapotranspiration induces an anomalous low-level cyclone centered over the eastern edge of the continent, bringing warm, moist air from the Gulf of Mexico and Caribbean northward along the coast of North America (figure S9). The transport of moisture into the wake region by this anomalous circulation damps the temperature-induced intensification of the RH wake. The combination of the opposing effects of the T and q changes on RH produces a slight intensification of the RH wake with increased bgcCO_2 across all models (figure 5).

The drivers of winter W_{RH} change are different than those in summer. In winter, there is little change in continental RH, but W_{RH} still intensifies (figure 3). Rather than being driven directly by downwind transport of anomalous continental RH, the reduction in winter W_{RH} is due to increased continental temperatures, which are caused by a darker land surface resulting from reduced snow cover and increased winter leaf area (figures S7 and S10). The darkened land

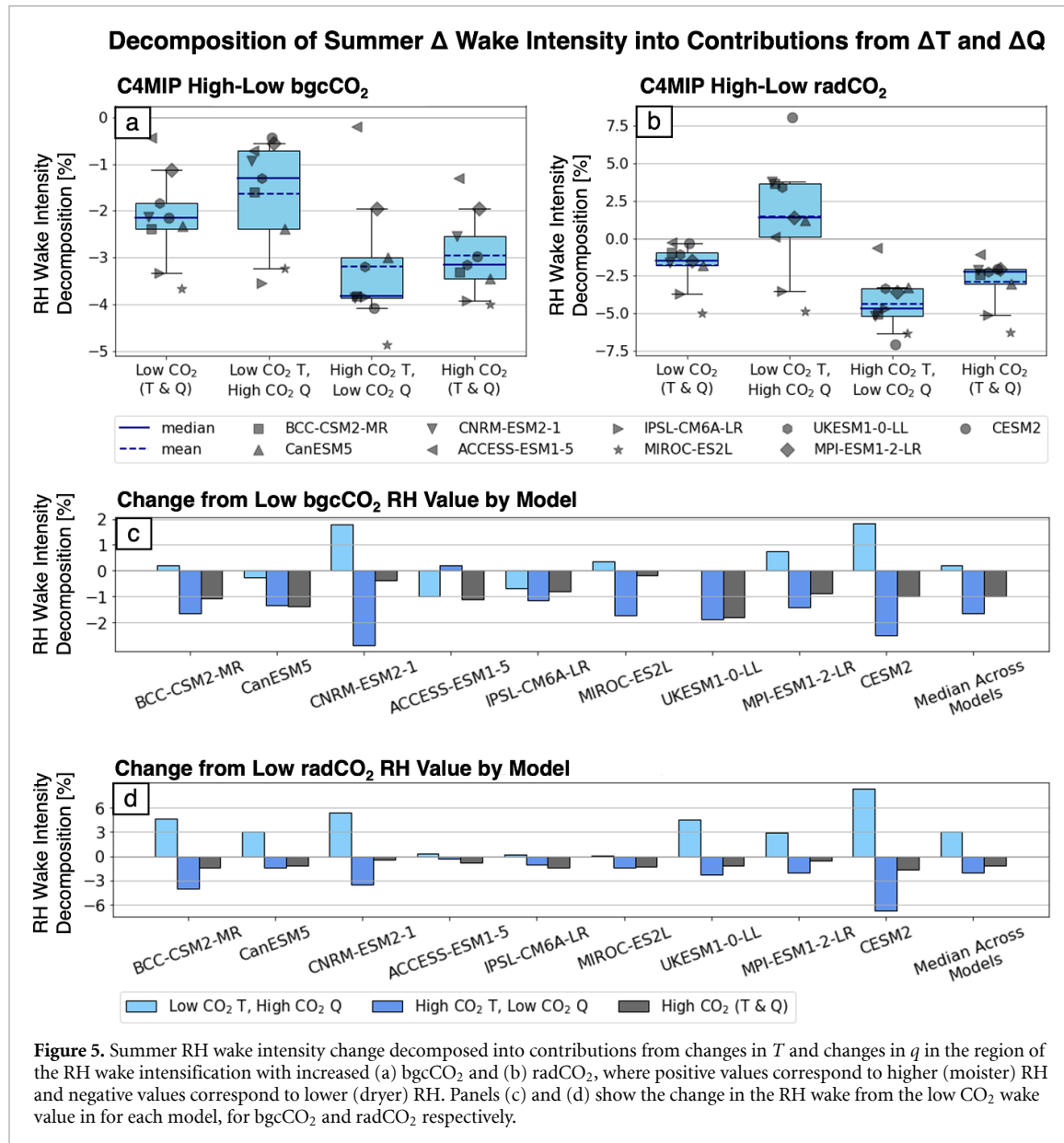


Figure 5. Summer RH wake intensity change decomposed into contributions from changes in T and changes in q in the region of the RH wake intensification with increased (a) bgcCO_2 and (b) radCO_2 , where positive values correspond to higher (moister) RH and negative values correspond to lower (drier) RH. Panels (c) and (d) show the change in the RH wake from the low CO_2 wake value in for each model, for bgcCO_2 and radCO_2 respectively.

surface absorbs more shortwave energy, leading to warming of the surface and overlying atmosphere in the winter.

3.4. Radiative effects of CO_2 intensify wake through continental warming

The radiative effects of enhanced CO_2 intensify W_{RH} in both winter and summer, but with spatial patterns and magnitudes that differ greatly from those caused by the biogeophysical effects of CO_2 (figure 3). The intensification of W_{RH} with increased radCO_2 results from the radiatively driven increase in land surface temperatures (figure S11). In contrast to increased bgcCO_2 , which has the largest impact on temperatures over land, increased radCO_2 drives widespread warming over both land and ocean, with stronger warming than bgcCO_2 ; the hotter atmosphere has a greater evaporative demand and causes increased terrestrial evapotranspiration in many regions (figure S11). This response of

evapotranspiration is not large enough to fill the enhanced vapor pressure deficit that drives it, so the large increase in land temperatures produces a decrease in summer continental RH and an intensification of W_{RH} . As in the bgcCO_2 case, q increases in the region where W_{RH} intensifies as a result of anomalous poleward winds over the western Atlantic, but for radCO_2 this poleward flow is part of an anomalous anticyclone centered over Florida and the Gulf of Mexico (figure S9). On its own, this increase in q would lead to a weaker W_{RH} , while the increase in T would lead to a strong intensification of W_{RH} (figure 5). The final result is a modest intensification of the wake as a result of increased radCO_2 .

While the peak magnitude of the wintertime W_{RH} change is more than twice as large for radCO_2 than for bgcCO_2 , the wake change induced by bgcCO_2 occupies a larger spatial area (cf figures 3(a) and (c)). In summer, the radCO_2 wake changes are largest in Hudson Bay and the Gulf of Mexico, while for bgcCO_2

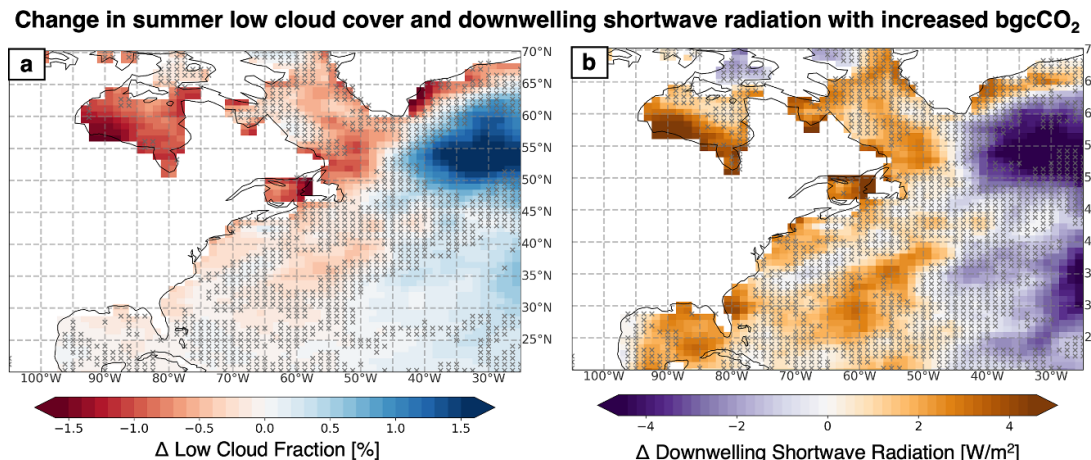


Figure 6. Change in summer low cloud fraction (left, %) and downwelling shortwave radiation at the surface (right, W m^{-2}) with increased bgcCO₂. Hatching indicates where less than 6/8 models agree on the sign of the response. ‘Low clouds’ are considered to be clouds from the surface to 700 hPa for models that report cloud fraction on pressure coordinates, and from the surface to 3000 m for models that report cloud fraction on height coordinates.

the changes occur largely along the eastern seaboard of Canada and the USA, suggesting that future plant changes driven by the biogeophysical effects of CO₂ will dominate changes in the wake from Florida to Newfoundland.

3.5. Implications for coastal clouds and radiation

Increased CO₂ drives changes not only in coastal RH, but in coastal cloud cover and radiation. With increased bgcCO₂, summer low cloud cover decreases along the full length of North America’s east coast, from the Gulf of Mexico to Hudson Bay (figure 6(a)). The reduced cloud fraction occurs year-round, with some seasonal changes in structure; cloud loss in the Gulf of Mexico is largest in winter (not shown), while cloud loss in Hudson Bay is largest in summer. Co-located with the reduction in low cloud cover is an increase of roughly 3 W m^{-2} in downwelling shortwave radiation (figure 6(b)). Coastal low cloud cover is also reduced as a result of increased radCO₂, though for that forcing the total change in downwelling shortwave radiation at the surface is complicated by the response of clouds and other absorbers to the radiative effects of CO₂ (not shown).

4. Discussion

The reduction in coastal cloud cover with increased bgcCO₂ is notable as the North American east coast is host to large human population centers and important marine ecosystems, in an area already prone to episodic clear-sky coastal events (figure S12). The changes in clouds directly alter the amount of sunlight reaching the ocean surface in these high-productivity coastal areas; while these regions are largely nutrient limited, they also experience seasonal light limitation (Arteaga *et al* 2014) and have high chlorophyll concentrations (Gregg *et al* 2005).

Thus, the response of the terrestrial carbon cycle to increased bgcCO₂ could, by altering downwelling shortwave radiation in the land wake region, impact ocean biogeochemistry.

Independent of its effects on ocean biology, increased ocean surface shortwave radiation also has implications for sea surface temperatures. While these changes in coastal cloud fraction and downwelling shortwave radiation are modest in magnitude, they represent an as-yet unidentified mechanism through which terrestrial processes—i.e. the plant response to bgcCO₂—can alter ocean processes by causing atmospheric change.

The biogeochemically induced changes in the land wake presented here represent a new mechanism of regional climate change. The radiative effects of increased atmospheric CO₂ on atmospheric water vapor and cloud cover have been widely examined, yet continue to be a large source of uncertainty for future climate projections (Held and Soden 2000, Stephens 2005, Lohmann 2006, Sherwood *et al* 2010, Wood 2012, Ceppli *et al* 2017, Kärcher 2017). The land wake represents a non-local climate response driven by the advection of air carrying a continental signature over ocean regions. This is distinct from changes in terrestrial climate driven by plant responses to CO₂ (e.g. Swann *et al* 2016, Zarakas *et al* 2020b) or vegetation change (e.g. Kleidon *et al* 2000), and distinct from large scale circulation-inducing ecoclimate teleconnections (e.g. Swann *et al* 2012, Garcia *et al* 2016, Laguë 2016).

The remote influence of continental biogeophysical and biogeochemical changes on oceanic air likely involve a related set of complex processes, with the changes in coastal temperatures and humidities coupled to the Plank, water vapor, and lapse rate feedbacks (Soden and Held 2006, Laguë *et al* 2021). These processes merit further exploration, in the context of

both forced long-term climate change and ongoing interannual variability.

Future study could also explore how extreme continental drought, heat waves, irrigation, and agriculture impact the land wake downwind of North America and other continents, and how terrestrially-driven atmospheric changes over ocean regions downwind of the continents impact ocean processes and productivity. The sensitivity of the wake to land-atmosphere coupling has yet to be explored. We might expect changes in terrestrial processes in regions with weak land-atmosphere coupling (e.g. as defined in Koster *et al* 2006) to have less impact on the continental wake than changes in terrestrial regions with strong land-atmosphere coupling. Further study should focus on which continental regions have the strongest control on the continental wake.

While this study focused on the Atlantic wake east of North America, similar mid-latitude wakes exist off the east coasts of Asia and South America (not shown). Asymmetries in RH also occur at lower latitudes, co-located with the subtropical cloud decks; further study is required to determine the relative contributions of ocean upwelling, atmospheric subsidence, clouds, and continental advection in these climatically important regions. Reanalysis data could be leveraged to explore the interannual variability of the wake and determine its sensitivity to large-scale climate modes of variability.

Data availability statement

ERA5 and C4MIP data are publicly available from <https://cds.climate.copernicus.eu/#!/search?text = ERA5&type = dataset> and <https://esgf-node.llnl.gov/projects/cmip6/>, respectively. Scripts used in the analysis, including the python environment used for analysis, are available on Zenodo at <https://doi.org/10.5281/zenodo.7153500>. No new data were created or analysed in this study.

Acknowledgments

This research used resources of the National Energy Research Scientific Computing Center (NERSC), a U.S. Department of Energy Office of Science User Facility located at Lawrence Berkeley National Laboratory, operated under Contract No. DE-AC02-05CH11231. We acknowledge high-performance computing support from Cheyenne ([10.5065/D6RX99HX](#)) provided by NCAR's Computational and Information Systems Laboratory, sponsored by the National Science Foundation, and the data access and computing support provided by the NCAR CMIP Analysis Platform ([10.5065/D60R9MSP](#)). We acknowledge the World Climate Research Programme, which, through its Working Group on Coupled Modelling, coordinated and promoted CMIP6. We thank the climate modeling groups for

producing and making available their model output, the Earth System Grid Federation (ESGF) for archiving the data and providing access, and the multiple funding agencies who support CMIP6 and ESGF. We acknowledge the use of imagery from the NASA Worldview application (<https://worldview.earthdata.nasa.gov/>), part of the NASA Earth Observing System Data and Information System (EOSDIS). M M L acknowledges funding support from the James S. McDonnell Foundation Postdoctoral Fellowship in Dynamic and Multiscale Systems. W R B acknowledges support by the U.S. Department of Energy, Office of Science, Office of Biological and Environmental Research, Climate and Environmental Sciences Division, Regional and Global Model Analysis Program, under Award DE-SC0019367.

Author contributions statement

M M L came up with the initial project idea, performed model simulations, and conducted the analysis. All authors discussed the analysis, suggested ideas for exploration, and contributed to the manuscript.

ORCID iDs

Marysa M Laguë  <https://orcid.org/0000-0001-8513-542X>
Gregory R Quentin  <https://orcid.org/0000-0002-7884-5332>
William R Boos  <https://orcid.org/0000-0001-9076-3551>

References

- Arteaga L, Pahlow M and Oschlies A 2014 Global patterns of phytoplankton nutrient and light colimitation inferred from an optimality-based model *Glob. Biogeochem. Cycles* **28** 648–61
Ball J T, Woodrow I E and Berry J A 1987 A model predicting stomatal conductance and its contribution to the control of photosynthesis under different environmental conditions *Progress in Photosynthesis Research* (Dordrecht: Springer)
Bathiany S, Claussen M, Brovkin V, Raddatz T and Gayler V 2010 Combined biogeophysical and biogeochemical effects of large-scale forest cover changes in the MPI earth system model *Biogeosciences* **7** 1383–99
Bergeron T 1930 Richtlinien einer dynamischen Klimatologie *Meteorol. Z.* **47** 246–62
Bonan G B 2008 Forests and climate change: Forcings, feedbacks and the climate benefits of forests *Science* **320** 1444–9
Bonan G B, Pollard D and Thompson S L 1992 Effects of boreal forest vegetation on global climate *Nature* **359** 716–8
Boos W R and Kuang Z 2013 Sensitivity of the South Asian monsoon to elevated and non-elevated heating *Sci. Rep.* **3** 3–6
Burke C J 1945 Transformation of polar continental air to polar maritime air *J. Meteorol.* **2** 94–112
Businger S and Reed R J 1989 Cyclogenesis in cold air masses *Weather Forecast.* **4** 133–56
Campbell J L, Mitchell M J, Groffman P M, Christenson L M and Hardy J P 2005 Winter in northeastern North America: a critical period for ecological processes *Front. Ecol. Environ.* **3** 314–22

- Carlson T N and Prospero J M 1972 The large-scale movement of Saharan air outbreaks over the Northern equatorial Atlantic *J. Appl. Meteorol.* **11** 283–97
- Ceppi P, Brent F, Zelinka M D and Hartmann D L 2017 Cloud feedback mechanisms and their representation in global climate models *Wiley Interdiscip. Rev.: Clim. Change* **8** e465
- Cess R D and Goldenberg S D 1981 The effect of ocean heat capacity upon global warming due to increasing atmospheric carbon dioxide *J. Geophys. Res.* **86** 498–502
- Chadwick R, Ackerley D, Ogura T and Dommenget D 2019 Separating the influences of land warming, the direct CO₂ effect, the plant physiological effect and SST warming on regional precipitation changes *J. Geophys. Res.* **124** 624–40
- Cheng L, Zhang L, Wang Y-P, Yu Q and Eamus D 2014 Quantifying the effects of elevated CO₂ on water budgets by combining FACE data with an ecohydrological model: quantifying the effects of elevated CO₂ on water budgets *Ecohydrology* **7** 1574–88
- Cook K H and Held I M 1992 The stationary response to large-scale orography in a general circulation model and a linear model *J. Atmos. Sci.* **49** 525–39
- Davin E L, de Noblet-Ducoudré N, de Noblet-Ducoudré N and de Noblet-Ducoudré N 2010 Climatic impact of global-scale deforestation: radiative versus nonradiative processes *J. Clim.* **23** 97–112
- Dong B, Gregory J M and Sutton R T 2009 Understanding land-sea warming contrast in response to increasing greenhouse gases. Part I: transient adjustment *J. Clim.* **22** 3079–97
- Donohue R J, Roderick M L, McVicar T R and Farquhar G D 2013 Impact of CO₂ fertilization on maximum foliage cover across the globe's warm, arid environments *Geophys. Res. Lett.* **40** 3031–5
- Eamus D 1991 The interaction of rising CO₂ and temperatures with water use efficiency *Plant, Cell Environ.* **14** 843–52
- Eyring V, Sandrine Bony G A Meehl C A Senior B S, Stouffer R J and Taylor K E 2016 Overview of the coupled model intercomparison project phase 6 (CMIP6) experimental design and organization *Geosci. Model Dev.* **9** 1937–58
- Field C B, Jackson R B and Mooney H A 1995 Stomatal responses to increased CO₂: implications from the plant to the global scale *Plant, Cell Environ.* **18** 1214–25
- Friedlingstein P et al 2006 Climate-carbon cycle feedback analysis: results from the C 4 MIP model intercomparison *J. Clim.* **19** 3337–53
- Fu J, Wang B, Chen Y and Ma Q 2018 The influence of continental air masses on the aerosols and nutrients deposition over the western North Pacific *Atmos. Environ.* **172** 1–11
- Fu Q and Feng S 2014 Responses of terrestrial aridity to global warming *J. Geophys. Res.* **119** 7863–75
- Fuchs J, Cermak J, Andersen H, Hollmann R and Schwarz K 2017 On the influence of air mass origin on low-cloud properties in the Southeast Atlantic *J. Geophys. Res.* **122** 11076–91
- Gannon P T 1978 *Influence of Earth Surface and Cloud Properties on the South Florida sea Breeze* ERL 402-NHEML 2 (Environmental Research Laboratories, National Oceanic and Atmospheric Administration, U.S. Department of Commerce)
- Garcia E S, Swann A L S, Villegas J C, Breshears D D, Law D J, Saleska S R and Stark S C 2016 Synergistic ecoclimate teleconnections from forest loss in different regions structure global ecological responses *PLoS One* **11** 1–12
- Garrett T J and Hobbs P V 1995 Long-range transport of continental aerosols over the Atlantic ocean and their effects on cloud structures *J. Atmos. Sci.* **52** 2977–84
- Gille S T, Smith S G L and Staton N M 2005 Global observations of the land breeze *Geophys. Res. Lett.* **32** 1–4
- Gregg W W, Casey N W and McClain C R 2005 Recent trends in global ocean chlorophyll *Geophys. Res. Lett.* **32** 1–5
- Harris C R et al 2020 Array programming with NumPy *Nature* **585** 357–62
- Hartmann D L 2016 *Global Physical Climatology* 2nd edn, vol 103 (Amsterdam: Elsevier)
- Held I M and Soden B J 2000 Water vapor feedback and global warming *Annu. Rev. Energy Environ.* **25** 441–475
- Held I M, Ting M and Wang H 2002 Northern winter stationary waves: theory and modeling *J. Clim.* **15** 2125–44
- Hersbach H et al 2020 The ERA5 global reanalysis *Q. J. R. Meteorol. Soc.* **146** 1999–2049
- Hoyer S and Hamman J 2017 xarray: N-D labeled arrays and datasets in Python *J. Open Res. Softw.* **5** 10
- IPCC 2007 Contribution of working group I to the fourth assessment report of the intergovernmental panel on climate change: summary for policymakers *Technical Report*
- IPCC 2022 *Global Warming of 1.5 °C: IPCC Special Report on Impacts of Global Warming of 1.5 °C Above Pre-Industrial Levels in Context of Strengthening Response to Climate Change, Sustainable Development and Efforts to Eradicate Poverty* 1st edn (Cambridge: Cambridge University Press)
- Jones C D et al 2016 C4MIP—the coupled climate-carbon cycle model intercomparison project: experimental protocol for CMIP6 *Geosci. Model Dev.* **9** 2853–80
- Kalkstein L S, Nichols M C, David Barthel C and Scott Greene J 1996 A new spatial synoptic classification: application to air-mass analysis *Int. J. Climatol.* **16** 983–1004
- Kärcher B 2017 Cirrus clouds and their response to anthropogenic activities *Curr. Clim. Change Rep.* **3** 45–57
- Kleidon A, Fraedrich K and Heimann M 2000 A green planet versus a desert world: estimating the maximum effect of vegetation on the land surface climate *Clim. Change* **44** 471–93
- Kooperman G J, Chen Y, Hoffman F M, Koven C D, Lindsay K, Pritchard M S, Swann A L S and Randerson J T 2017 Forest response to rising CO₂ drives zonally asymmetric rainfall change over tropical continents *Nat. Clim. Change* **8** 1–36
- Koster R D et al 2006 GLACE: the global land-atmosphere coupling experiment. Part I: overview *J. Hydrometeorol.* **7** 590–610
- Laguë M M 2016 Progressive mid-latitude afforestation: local and remote climate impacts in the framework of two coupled earth system models *Master's Thesis* (Seattle, WA: University of Washington)
- Laguë M M, Bonan G B and Swann A L S 2019 Separating the impact of individual land surface properties on the terrestrial surface energy budget in both the coupled and uncoupled land-atmosphere system *J. Clim.* **32** 5725–44
- Laguë M M and Swann A L S 2016 Progressive midlatitude afforestation: impacts on clouds, global energy transport and precipitation *J. Clim.* **29** 5561–73
- Laguë M M, Swann A L S and Boos W R 2021 Radiative feedbacks on land surface change and associated tropical precipitation shifts *J. Clim.* **34** 1–63
- Li C and Yanai M 1996 The onset and interannual variability of the Asian summer monsoon in relation to land-sea thermal contrast *J. Clim.* **9** 358–75
- Lohmann U 2006 Aerosol effects on clouds and climate *Space Sci. Rev.* **125** 129–37
- Maroon E A, Frierson D M W and Battisti D S 2015 The tropical precipitation response to Andes topography and ocean heat fluxes in an aquaplanet model *J. Clim.* **28** 381–98
- Medlyn B E et al 2001 Stomatal conductance of forest species after long-term exposure to elevated CO₂ concentration: a synthesis *New Phytol.* **149** 247–64
- Medlyn B E, Duursma R A, Eamus D, Ellsworth D S, Prentice I C, Barton C V, Crous K Y, De Angelis P, Freeman M and Wingate L 2011 Reconciling the optimal and empirical approaches to modelling stomatal conductance *Glob. Change Biol.* **17** 2134–44
- Morison J I L 2001 Increasing atmospheric CO₂ and stomata *New Phytol.* **149** 154–6
- Myneni R B, Los S O and Tucker C J 1966 Satellite-based identification of linked vegetation index and sea surface temperature anomaly areas from 1982–1990 for Africa, Australia and South America *Geophys. Res. Lett.* **23** 729–32

- Nilsson E D, Paatero J and Boy M 2001 Effects of air masses and synoptic weather on aerosol formation in the continental boundary layer *Tellus B* **53** 462–78
- North G R, Mengel J G and Short D A 1983 Simple energy balance model resolving the seasons and the continents: Application to the astronomical theory of the ice ages *J. Geophys. Res.* **88** 6576–86
- O’Gorman P A and Muller C J 2010 How closely do changes in surface and column water vapor follow Clausius-Clapeyron scaling in climate change simulations? *Environ. Res. Lett.* **5** 025207
- Palmén E 1951 The aerology of extratropical disturbances *Compendium of Meteorology* ed T F Malone (Boston, MA: American Meteorological Society) pp 599–620
- Parrish D D, Hahn C J, Williams E J, Norton R B, Fehsenfeld F C, Singh H B, Shetter J D, Gandrud B W and Ridley B A 1992 Indications of photochemical histories of Pacific air masses from measurements of atmospheric trace species at Point Arena, California *J. Geophys. Res. Atmos.* **97** 15883–901
- Perry S J, McGregor S, Sen Gupta A and England M H 2017 Future changes to El Niño-Southern oscillation temperature and precipitation teleconnections *Geophys. Res. Lett.* **44** 10,608–16
- Pithan F, Svensson G, Caballero R, Dmitry Chechin T W Cronin A M L Ekman R N, Shupe M D, Solomon A, Tjernström M and Wendisch M 2018 Role of air-mass transformations in exchange between the Arctic and mid-latitudes *Nat. Geosci.* **11** 805–12
- Robertson F R, Bosilovich M G and Roberts J B 2016 Reconciling land-ocean moisture transport variability in reanalyses with P - ET in observationally driven land surface models *J. Clim.* **29** 8625–46
- Schwartz M D 1991 An integrated approach to air mass classification in the North Central United States *Prof. Geogr.* **43** 77–91
- Schwartz M D 1995 Detecting structural climate change: an air mass-based approach in the North Central United States, 1958–1992 *Ann. Assoc. Am. Geogr.* **85** 553–68
- Sellers P J et al 1996 Comparison of radiative and physiological effects of doubled atmospheric CO₂ on climate *Science* **271** 1402–5
- Shaw T A and Voigt A 2016 Land dominates the regional response to CO₂ direct radiative forcing *Geophys. Res. Lett.* **43** 11,383–91
- Sherwood S C, Roca R, Weckwerth T M and Andronova N G 2010 Tropospheric water vapor, convection and climate *Rev. Geophys.* **48** 1–29
- Soden B J and Held I M 2006 An assessment of climate feedbacks in coupled ocean-atmosphere models *J. Clim.* **19** 3354–60
- Sonu C J, Murray S P, Hsu S A, Suhayda J N and Waddell E 1973 Sea Breeze and coastal processes EOS, *Trans. Am. Geophys. Union* **54** 820–33
- Stephens G L 2005 Cloud feedbacks in the climate system: a critical review *J. Clim.* **18** 237–73
- Sutton R T, Dong B and Gregory J M 2007 Land/sea warming ratio in response to climate change: IPCC AR4 model results and comparison with observations *Geophys. Res. Lett.* **34** 2–6
- Swann A L S, Fung I Y, John C H Chiang H 2012 Mid-latitude afforestation shifts general circulation and tropical precipitation *Proc. Natl Acad. Sci.* **109** 712–6
- Swann A L S, Hoffman F M, Koven C D and Randerson J T 2016 Plant responses to increasing CO₂ reduce estimates of climate impacts on drought severity *Proc. Natl Acad. Sci.* **113** 10019–24
- White R H, Battisti D S and Roe G H 2017 Mongolian mountains matter most: impacts of the latitude and height of Asian orography on Pacific wintertime atmospheric circulation *J. Clim.* **30** 4065–82
- Willett H C 1933 *American Air Mass Properties Papers in Physical Oceanography and Meteorology* vol 2 (Cambridge, MA: Massachusetts Institute of Technology) p 117
- Wood R 2012 Stratocumulus clouds *Mon. Weather Rev.* **140** 2373–423
- Wu G, Liu Y, Bian H, Bao Q, Duan A and Jin F F 2012 Thermal controls on the asian summer monsoon *Sci. Rep.* **2** 1–7
- Yang X and Delsole T 2012 Systematic comparison of ENSO teleconnection patterns between models and observations *J. Clim.* **25** 425–46
- Zarakas C M, Swann A L S, Laguë M M, Armour K C and Randerson J T 2020 Plant physiology increases the magnitude and spread of the transient climate response to CO₂ in CMIP6 Earth system models *J. Clim.* **33** 8561–78
- Zarakas C M, Swann A L, Laguë M M, Armour K C and Randerson J T 2020 Plant physiology increases the magnitude and spread of the transient climate response to CO₂ in CMIP6 Earth system models *J. Clim.* **33** 8561–78